Migration and deposition of ^{13}C in the full-tungsten ASDEX Upgrade tokamak

A Hakola[1,2]‡, J Likonen[2], L Aho-Mantila[1], M Groth[1], S Koivuranta[2], K Krieger[3], T Kurki-Suonio[1], T Makkonen[1], M Mayer[3], H W Müller[3], R Neu[3], V Rohde[3] and the ASDEX Upgrade Team

[1] Department of Applied Physics, Helsinki University of Technology, Association EURATOM-Tekes, P.O. Box 4100, FI-02015 TKK, Finland

[2] VTT Materials for Power Engineering, Association EURATOM-Tekes, P.O. Box 1000, FI-02044 VTT, Finland

[3] Max-Planck-Institut für Plasmaphysik, EURATOM Association, Boltzmannstrasse 2, D-85748 Garching, Germany

E-mail: antti.hakola@tkk.fi

Abstract. The migration of carbon in low-density, low-confinement plasmas of ASDEX Upgrade was studied by injecting ^{13}C into the main chamber of the torus at the end of the 2007 experimental campaign. A selection of standard tungsten-coated lower-divertor and main-chamber tiles as well as a complete set of lower-divertor tiles with an uncoated poloidal marker stripe were removed from one poloidal cross section and analyzed using secondary ion mass spectrometry (SIMS). The poloidal deposition profiles of ^{13}C on both the tungsten-coated tiles and on the uncoated graphite areas of the marker tiles were measured and compared. For the W-coated lower-divertor tiles, ^{13}C was deposited mainly on the high-field side tiles, while barely detectable amounts of ^{13}C were observed on low-field side samples. In contrast, on the uncoated marker stripes the deposition was equally pronounced in the high-field and low-field side divertor. The marker-tile results are in agreement with those obtained from graphite tiles after the 2003 and 2005 ^{13}C experiments in ASDEX Upgrade. In the case of W-coated tiles, the ^{13}C measurements were complemented by determining the total amount of deposited carbon (^{12}C) on the tiles, which also shows strong deposition at the inner parts of the lower divertor. The estimated deposition of ^{13}C on W at the divertor areas was less than 1.5% of the injected amount of ^{13}C atoms. The ^{13}C analyses of the main-chamber tiles and small silicon samples mounted in remote areas revealed significant deposition in the upper divertor, in upper parts of the heat shield, in the limiter region close to the injection valve, and below the roof baffle. Approximately 8% of the injected ^{13}C is estimated to have accumulated in these regions. Possible reasons for the different deposition patterns on W and on graphite in different regions of the torus are discussed.

PACS numbers: 52.40.Hf, 52.55.Fa, 52.55.Rk, 68.49.Sf, 82.80.Ms

‡ Corresponding author.

Submitted to: *Plasma Phys. Control. Fusion*

1. Introduction

The successful operation of ITER sets stringent requirements for the materials used in its critical plasma-facing components (PFCs). The current consensus, at least for the initial phase of ITER, is to use beryllium in the main chamber, tungsten in the divertor, and carbon-fibre composite (CFC) in the strike-point regions [1–3]. Carbon (C) is a favourable material in present tokamaks since it mainly radiates in the scrape-off layer (SOL), is particularly resistant to thermal shocks and tolerates high power loads that might occur during ELMs and disruptions. However, it suffers from significant chemical erosion even at low plasma temperatures [4, 5], and co-deposition of the eroded carbon with hydrogen isotopes may lead to high tritium inventories in the wall structures [6, 7]. Furthermore, the deposited carbon layers have the unfavourable property of disintegrating into dust in the reactor [8]. Beryllium (Be), for its part, is a light element with adequate thermal properties. It is also expected to radiate power only at the plasma edge and act as an effective oxygen getter [9]. Unfortunately, Be will erode to a high degree under reactor conditions and the retention of tritium in beryllium is an important issue albeit the retention rate is expected to be lower than in the case of carbon [2, 6].

In contrast, tungsten (W) is not eroded as heavily as beryllium or carbon and the accumulation of tritium in bulk W is small [2, 4–6]. The biggest drawback in using tungsten is, however, that even small amounts of W eroded from the wall can result in significant radiation in the core plasma, which, in turn, prevents high plasma performance. Despite this restriction, tungsten has proven to be a suitable alternative to conventionally used carbon as the main first-wall material [10–12]. ASDEX Upgrade has been pioneering with tungsten PFCs since 1999. The tungsten coverage of its first wall has been gradually increased, and by the beginning of the 2007 experimental campaign, all the first-wall tiles had been replaced with tungsten-coated ones.

During the transition period from a carbon-dominated to a full-tungsten ASDEX Upgrade, the erosion of PFCs as well as the migration of different elements and their subsequent deposition on new locations has been extensively studied. The investigations have mainly been based on *post mortem* surface analysis of wall tiles or long-term probes after an experimental campaign. Various ion-beam techniques such as Rutherford backscattering (RBS), nuclear reaction analysis (NRA), and secondary ion mass spectrometry (SIMS) have been used for this purpose. Particularly, the changes in the erosion and deposition profiles of carbon and tungsten and in the inventory of deuterium in wall tiles have been determined. The main campaign-integrated experimental results can be summarized in the following:

- The outer (low-field side) divertor, especially regions close to the outer strike point, is a net erosion area for both C and W [14–16].
- The inner (high-field side) divertor is a net carbon deposition area and deposition there exceeds erosion in the outer divertor due to additional C sources in the main chamber [14, 17]. After the transition to the full-W machine, the amount

of deposited carbon that remains inside the torus has been significantly reduced and the poloidal deposition pattern has changed [18].

- The inner divertor is a net deposition area also for W but only a small fraction of the tungsten eroded in the main chamber and outer divertor ends up in the re-deposited layers in the inner divertor [16].
- The retention of deuterium in the PFCs in the carbon phase was dominated by co-deposition of hydrogen isotopes with carbon in the inner divertor and remote areas [19]. In the tungsten phase, the amount of retained deuterium has been reduced by a factor of 5–10. Both co-deposition in the inner divertor and implantation and trapping in the W coatings in the outer divertor contribute to the deuterium inventories [18].

Similar results of the erosion/deposition asymmetry and retention of deuterium have been obtained in other tokamaks, e.g., in JET [20, 21] and in Tore Supra [22, 23].

The main limitation with the campaign-integrated post-mortem data is that the observed erosion and deposition patterns have been formed as a result of PFCs exposed to numerous plasma discharges, including different plasma configurations, confinement and divertor detachment regimes, and regular openings of the vacuum vessel. To better understand the migration mechanisms of the key elements and to obtain unambiguous data for modelling purposes, the long-term analyses have to be supplemented by, e.g., *ex situ* characterization of marker probes after their exposure to plasma during a pre-selected number of discharges or by applying different tracer techniques. Here, "tracer" refers to experiments where small quantities of a marker substance are deliberately injected into the machine during successive, identical plasma shots, and the distribution of this substance on PFCs around the torus is determined immediately after the experiment.

In ASDEX Upgrade, tracer injections have been carried out by puffing isotopically labelled methane ($^{13}CH_4$) into the torus just before venting and opening the vessel for maintenance work. ^{13}C has been selected as the marker element since it is a stable element and can easily be distinguished from the more abundant ^{12}C by standard surface-analysis techniques. This paper focuses on experiments in which $^{13}CH_4$ was puffed into the scrape-off layer at the outer midplane, as was done in ASDEX Upgrade in 2003, 2004, 2005, and 2007. After each experiment, a selection of wall tiles was analyzed using SIMS and the poloidal deposition profile of ^{13}C on them was determined [24, 25]. Similar marker-element injections have also been carried out in JET and DIII-D using either $^{13}CH_4$ or SiH_4 as the tracer agent [26–30]. During the last few years, much effort has been put on modelling the migration of ^{13}C and explaining the observed experimental results. Monte-Carlo-based impurity transport codes and fluid codes including DIVIMP, SOLPS, OEDGE, UEDGE, and EDGE2D have been used for these purposes [31–37]. Important migration pathways have been identified but modelling of the migration mechanisms, let alone complete understanding of the related physics, is still far behind to explain the experimental observations.

In this article, we have investigated using SIMS the deposition of ^{13}C on the first-wall tiles of ASDEX Upgrade after the 2007 injection experiment. The main goal is to compare the poloidal ^{13}C deposition profiles, particularly in the lower-divertor regions, determined from standard tungsten-coated ASDEX Upgrade tiles and from uncoated graphite stripes in marker tiles produced for the 2007 campaign. This way, the effect of substrate material (C on W vs. C on C) on the deposition behaviour of ^{13}C can be studied. In addition, the roughness and topography of the surfaces of selected samples were studied to investigate their roles in the deposition of ^{13}C; along with material, the surface quality has been observed to significantly alter the deposition efficiency of carbon [39–41]. The main results of the earlier ^{13}C injection experiments, performed during the carbon-dominated phase of ASDEX Upgrade, are also revisited and compared with the 2007 data. Complementary information about the deposition and migration behaviour of carbon is provided by the measured SIMS depth profiles of ^{12}C and the reported RBS/NRA results of accumulated carbon on the W coatings [18]. The details of the injection experiments as well as of the tile analysis are described in section 2. Section 3 presents the SIMS results of ^{13}C on tile surfaces and compares them with existing data. Also simulation efforts with the DIVIMP code are presented in the end of this section. In section 4, the SIMS data on long-term deposition of carbon is presented, and in section 5 the results are discussed and conclusions are drawn.

2. Experimental methods

2.1. ^{13}C experiments in ASDEX Upgrade

^{13}C in the form of isotopically labelled methane ($^{13}CH_4$) has been injected into ASDEX Upgrade from the outer (low-field side) midplane at the end of four experimental campaigns: 2002/2003, 2003/2004, 2004/2005, and 2007. This article concentrates on the 2007 experiment but, for comparison, the parameters and main results of all the ^{13}C experiments are summarized here. The three first experiments have been discussed in [24, 25], where also the relevant SIMS measurement data can be found.

In each experiment, puffing was done from one toroidal location in sector 9 during 10–15 identical plasma discharges either in H-mode (2003 and 2004) or in L-mode (2005 and 2007), typically with the lower single-null (LSN) plasma configuration except in 2004 when the upper single-null (USN) configuration was selected for upper-divertor studies. The main parameters of the different experiments are shown in table 1. The outlet of the gas valve was located 330 mm below the midplane and 250 mm to the left of the center line of the flange, and its radial position was 3444 mm; the radial positions of the closest wall tiles are around 2200 mm. The injection rate of methane was typically 1.0×10^{21} s^{-1} (except 2.0×10^{20} s^{-1} in 2004), and the flat-top time of each discharge was approximately 4.5 s during the 2003 and 2004 experiments, 7 s in 2005, and 3.5 s in 2007. The heating was usually done using neutral beam injection (NBI), but in 2007 NBI was applied only during the current ramp-up phase, and electron cyclotrone

Table 1. Main parameters of the different ^{13}C injection experiments. In the case of the 2007 experiment, the value in parentheses (3.4 MW) is the total auxiliary heating power during a discharge whereas 0.9 MW is the power applied during the flat-top phase.

Campaign	**Discharges/ configuration**	**Wall mat.**	**Gas**	$\mathbf{B_t}$ **(T)**	$\mathbf{I_p}$ **(MA)**	$\mathbf{n_e}$ **($\times 10^{19}$ m^{-3})**	$\mathbf{P_{aux}}$ **(MW)**	^{13}**C injected ($\times 10^{22}$ atoms)**
2007	22573–22585 L-mode, LSN	W	D	−2.5	0.8	3.3	0.9 (3.4)	2.7
2004/2005	20646–20659 L-mode, LSN	C/W	H	−2.5	0.8	6.0	2.9	5.0
2003/2004	19535–19546 H-mode, USN	C/W	H	−2.0	0.8	9.0	5.1	0.21
2002/2003	18190–18202 H-mode, LSN	C/W	H	−2.0	1.0	8.5	6.8	3.2

resonance heating (ECRH) was used after 1 s. During the flat-top phase, the auxiliary heating power by ECRH alone was $P_{\rm aux} = 0.9$ MW, while the total maximum heating power during the whole discharge was 3.4 MW.

The radial profiles of electron density ($n_{\rm e}$) and temperature ($T_{\rm e}$) across the separatrix at the outer midplane during constant plasma conditions for selected discharges of the three lower single-null experiments are shown in figure 1(a) and (b), respectively. The data is extracted from Thomson scattering, Li beam, and reflectometer measurements. One observes that in 2007 the electron density was clearly the lowest but the electron temperature much higher than in 2005, and the separatrix parameters were $n_{\rm e,sep} \approx 1 \times 10^{19}$ m^{-3} and $T_{\rm e,sep} \approx 20$ eV. Figure 1 also shows the ion saturation current ($j_{\rm sat}$), electron temperature ($T_{\rm e}$), and electron density ($n_{\rm e}$) along the outer (Figure 1(c)) and inner (Figure 1(d)) strike-point zones of the lower divertor, derived from Langmuir-probe data. In 2007, values around 20 eV were measured for $T_{\rm e}$ close to both the inner and outer strike points, indicating that the divertor plasmas were in the attached regime. In contrast, in 2005, $T_{\rm e}$ at the inner target was below 5 eV according to measurements indicating that the inner divertor plasma was in the high-recycling regime and likely to be detached.

When considering the two L-mode experiments, the following additional differences between them can be noticed: (i) the former experiment (2005) was done in hydrogen, while the latter (2007) in deuterium, (ii) the plasma density and the amount of puffed methane were approximately a factor of two smaller in 2007, (iii) no boronizations were made in 2007, and (iv) in 2007 the injections were done in a full-W environment; the wall tiles were carefully cleaned of all the previous deposition remnants before the campaign.

2.2. Wall materials

All the first-wall tiles of ASDEX Upgrade were replaced with tungsten-coated ones by the beginning of the 2007 campaign. The details of the tungsten programme and the

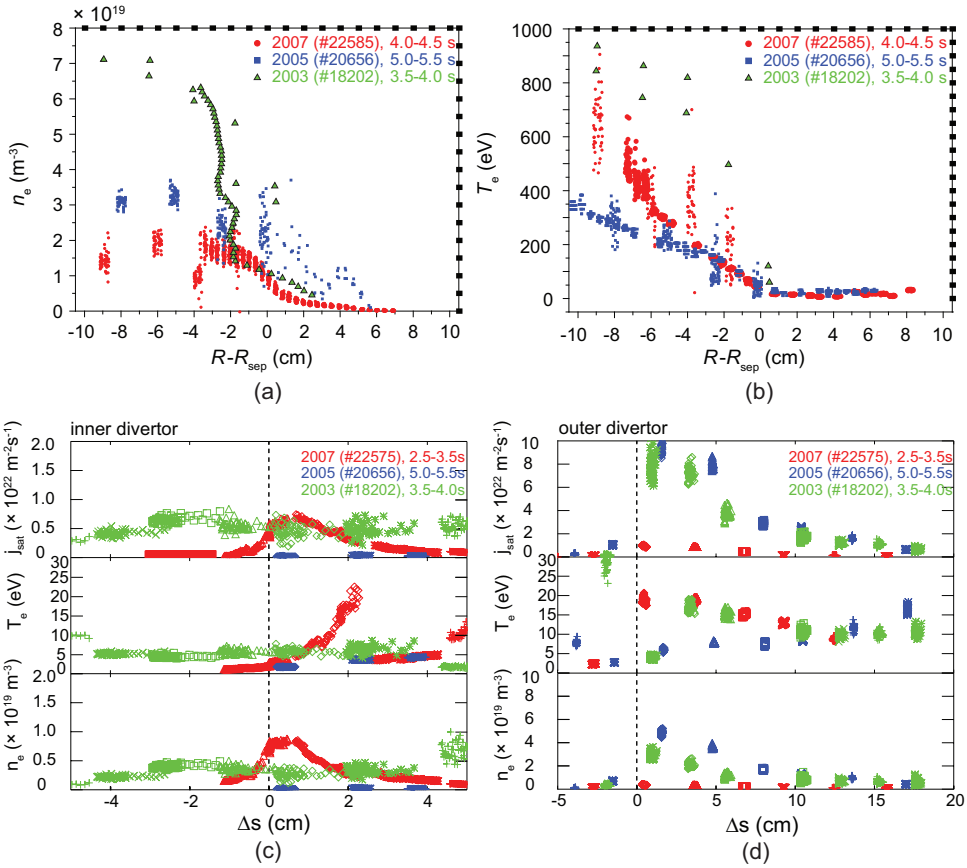

Figure 1. (a) Radial electron density profiles across the separatrix ($R - R_{\rm sep} = 0$) at the outer (low-field side) midplane for selected discharges of the 2003 (green triangles), 2005 (blue squares) and 2007 (red circles) experiments during the flat-top phases for the plasma current and density. (b) Corresponding electron temperature profiles for the same discharges. (c,d) Profiles of ion saturation current (top), electron temperature (middle), and electron density (bottom) along the inner strike-point (c) and outer strike-point regions (d). The dashed vertical lines denote the strike points, and $\Delta s < 0$ corresponds to the private flux region. The colour coding is green for the 2003, blue for the 2005, and red for the 2007 experiment. In (c) and (d), the discharge representing the 2007 experiment is different from that in (a) and (b), but the $n_{\rm e}$ and $T_{\rm e}$ profiles of the two discharges 22575 and 22585 are practically identical across the separatrix. The high $T_{\rm e}$ measured at private flux region in (d) during the 2003 experiment is probably unrealistic since $j_{\rm sat} = 0$ there.

locations of the W-coated tiles during each campaign can be found in [10, 13]. The tiles have graphite as their substrate material on which a 1–5-μm thick W film is deposited by physical vapour deposition (PVD). For the outer strike point tiles, the region where the highest heat and particle loads are expected, 200-μm thick W layers, produced using vacuum plasma spraying (VPS), have been used in 2007.

In addition to the standard tiles discussed above, a complete poloidal set of lower-divertor tiles with well-defined marker stripes on them was coated using an arc-discharge method [38] by DIARC-Technology Inc. before the 2007 campaign. The tiles relevant

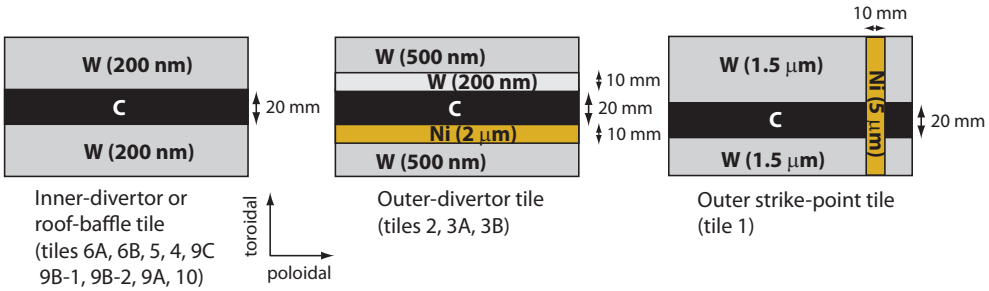

Figure 2. Schematic illustration of locations and widths of marker stripes in tiles prepared for the 2007 campaign. Tile labels correspond to those in figure 4

for the ^{13}C studies were mounted in one poloidal cross section of the sector 11 of the torus and they had the following specifications:

- All the inner-divertor and roof-baffle tiles had a 20-mm wide uncoated poloidal stripe in the middle and a 200-nm thick W coating on the remaining areas — excluding tile 4B below the inner strike point which only had the 200-nm W layer on it.
- The outer-divertor tiles had three adjacent poloidal stripes on them: an uncoated area (width 20 mm), a Ni marker (width 10 mm, thickness 2 μm), and a W marker (width 10 mm, thickness 200 nm). The nominal thickness of the remaining W coating of the tiles was 500 nm.
- The outer strike-point tile had an uncoated poloidal stripe (width 20 mm) and a toroidal Ni stripe (width 10 mm, thickness 5 μm) on top of everything close to the upper edge of the tile. The rest of the tile was coated with a 1.5-μm thick W film.

Small steps between the different marker stripes and regions do not have a major effect on the deposition behaviour of the elements of interest: the surface roughness of fresh marker coatings is typically much larger (of the order of several micrometers) than their thickness. A schematic illustration of the locations, widths, and materials of the marker stripes is shown in figure 2. Photographs of selected marker tiles (tiles 6A, 4, and 2) from inner and outer divertor regions after their plasma exposure in 2007 are shown in figure 3(a); the tile labels correspond to those in figure 4. Also the positions of samples drilled for SIMS analyses can be seen in the figure. Figure 3(b) shows photographs of slices cut from the corresponding PVD-coated tiles for SIMS analyses after the 2007 experiment.

2.3. Tile analysis

After the 2007 experiment, both the marker tiles and selected PVD/VPS-coated wall tiles from an adjacent poloidal cross section in sector 11 were removed for post-mortem surface analysis. The retrieved tiles were approximately 45 degrees toroidally separated from the injection valve in sector 9. The poloidal locations of the analyzed tiles are shown

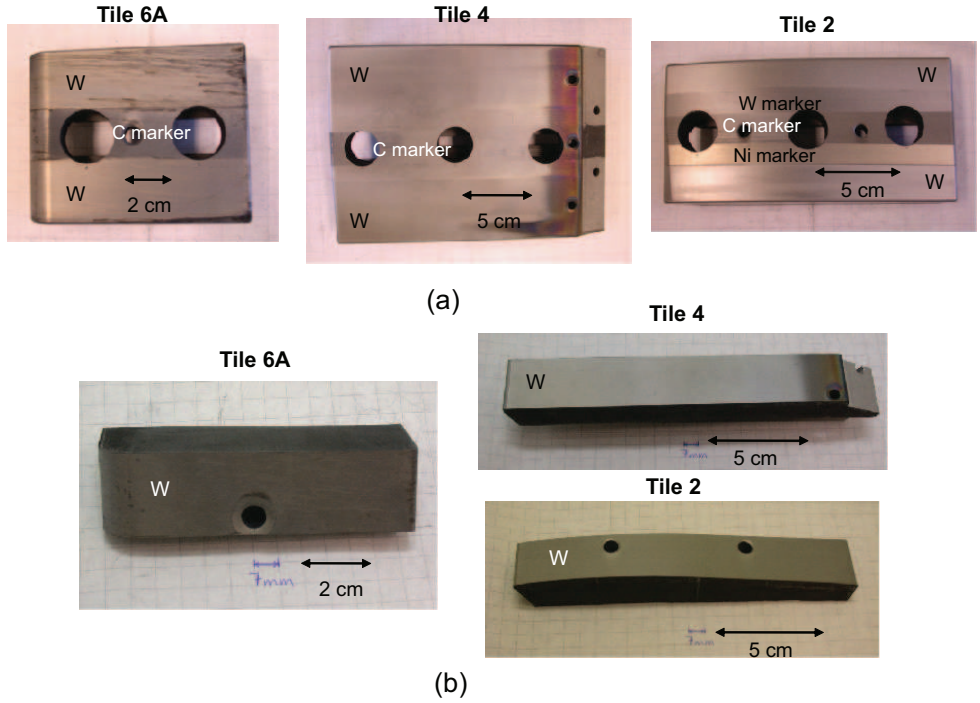

Figure 3. (a) Photographs of the marker tiles 6A (left), 4 (middle), and 2 (right) after their exposure to ASDEX Upgrade plasma in 2007. Tiles 6A and 4 are from the inner divertor and tile 2 from the outer divertor. The holes on the originally uncoated graphite areas mark the locations of the samples drilled for the SIMS analyses. Note the traces of arcing in tile 6A, a thick deposited layer close to the right edge of tile 4 (inner strike-point area) and thin W films on the uncoated C stripes (tiles 4 and 2). (b) Photographs of slices of PVD-coated tiles 6A (left), 4 (right, top) and 2 (right, bottom) after the 2007 campaign. A deposited layer can again be observed at the right edge of tile 4.

in figure 4. Similarly to the marker tiles, the W-coated lower-divertor tiles formed a complete set, whereas the main-chamber tiles originated from representative locations of the heat shield, the upper divertor, the passive stabilizer loop (PSL), and the limiter region of one of the cross sections (the limiter tile originated from sector 8). All the W-coated tiles were analyzed with SIMS and NRA. The marker tiles, for their part, were studied using SIMS and RBS. The SIMS results were used to evaluate the deposition of ^{13}C both on the tiles with the PVD/VPS tungsten coatings and on the uncoated stripes of the marker tiles, and to determine the inventory of carbon in tungsten. The NRA measurements provided quantitative data of the deposition of carbon in the coatings [18], and the RBS measurements performed before and after installing the marker tiles into ASDEX Upgrade revealed net erosion of the tungsten and nickel stripes and deposition on them [16]. In addition to the tiles, seven small silicon samples, three of which were mounted close to the injection valve and the rest below the roof baffle, were removed from the torus and analyzed to gather information on the deposition of ^{13}C in remote

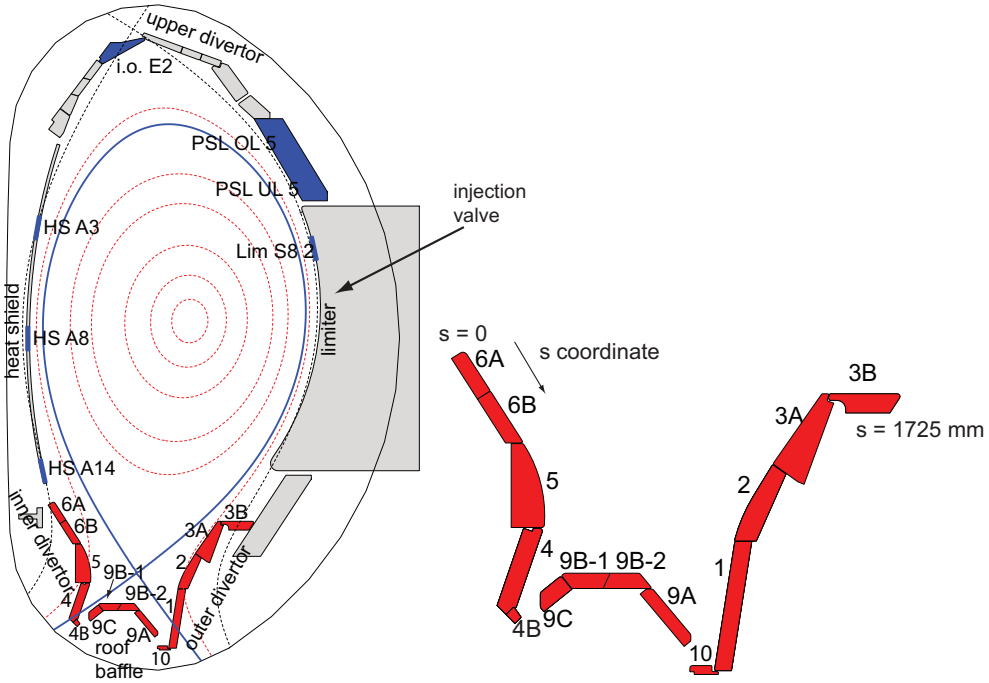

Figure 4. Illustration of a poloidal cross section of ASDEX Upgrade (left) and a magnification of the divertor area (right). The locations of the analyzed W-coated tiles are marked in red (divertor) or in blue (main chamber). Marker tiles were located only in the divertor region. The labels of the tiles and reference values for the s coordinate are given for further use. Also the separatrix (solid blue curve) and selected flux surfaces (dotted curves) for the discharge #22575 at 3.0 s are shown in the figure.

areas.

For the SIMS analyses, 1–5 cylindrical samples with a diameter of approximately 17 mm were drilled from each tile; the number of samples was chosen as large as practically possible to enable extensive deposition studies as a function of the poloidal s coordinate. The s coordinate starts from the innermost corner of the inner divertor (top edge of tile 6A in figure 4) and runs poloidally counter-clockwise around the torus along the tile surfaces. In each sample, the measurements were made at points located in two or three different rows, each corresponding to a different value for the s coordinate, and in every row the measurements were repeated 2–5 times. The W-coated samples were drilled from 25-mm wide slices cut from the central part of each tile whereas the marker-tile samples were taken from originally uncoated poloidal areas (see figure 2).

We used a double focussing magnetic sector SIMS (VG Ionex IX-70S), located at the Technical Research Centre of Finland (VTT), for the measurements. A 5-keV O_2^+ primary ion beam was applied, and the intensities (counts/s) of the emitted positive secondary ions at m/z values of 1 (H), 2 (D), 10 (B), 12 (^{12}C), 13 (^{13}C), and 184 (W) were profiled as functions of time. The current of the primary ions was adjusted to 500 nA during the profiling, and the beam was raster-scanned across an area of 300×430 μm^2. A 10-% electronic gate and a 1-mm optical gate were used in all the

measurements to eliminate the disturbing ejection of particles from the edges of the SIMS crater. The measurement time was converted to the depth of the studied spot by using the determined sputtering rates of 0.37 nm/s for the tungsten coating and 1.5 nm/s for the carbon substrate. These values were obtained by measuring the depths of a few SIMS craters with a profilometer (Dektak 3030ST, tip radius 2.5 μm). The profilometer was also used to determine the average surface roughness R_a (in nm) of selected W-coated and marker-tile samples. In addition, the surface topography of some SIMS samples was studied with a Hitachi S-4700 cold field emission electron gun scanning electron microscope (SEM). The images were taken by using a low acceleration voltage (5 kV) in order to enhance surface sensitivity.

For the ^{13}C analysis, a high mass resolution of $m/\Delta m = 2000$ at $m/z = 28$ was used to distinguish the elemental ^{13}C peak from closely lying isobars such as $^{12}CH^+$; the profiling of the selected elements in the whole W layer was done with coarser settings of $m/\Delta m \approx 300$. The amount of deposited ^{13}C on the sample surfaces and that of ^{12}C in the W coatings were evaluated by integrating the intensity of the corresponding mass signal down to the depth where the background level had been reached; the corresponding integral due to the ^{13}C background was subtracted from the results. Calibration samples with well-known surface densities (in at/cm^2) of ^{13}C on W or on C were used to transform the results into quantitative ones. When studying the overall deposition of ^{12}C in the W coatings, the NRA results provided the required calibration data. In the case of W-coated tiles, the intensity of the ^{13}C signal was normalized to that of tungsten whereas for the marker-tile samples, the normalization was done with respect to the ^{12}C signal.

3. Deposition of ^{13}C on tungsten and on carbon

3.1. ^{13}C on tungsten-coated tiles

On the W-coated tiles, the injected ^{13}C was typically deposited in a thin surface layer, and at the inner side of the divertor the ^{13}C levels were significantly larger than at the outer side. This can be seen in figure 5, where examples of SIMS depth profiles of ^{13}C from selected inner-divertor (6A, 6B, 5, and 4), roof-baffle (9B-1 and 9A), and outer-divertor tiles (1, 2, 3A, and 3B) are shown. The ^{13}C signal typically reaches its background level within the first 100 nm but one should note that the largest contribution comes from a 10–50 nm thick surface layer. In tiles 4, 6A, and 6B from the inner divertor, the ^{13}C signal behaves, however, somewhat differently: it shows an implantation-like profile and stays in a high level down to a depth of 100–200 nm. The ^{13}C profiles measured from the main chamber tiles were rather similar to the profiles taken from outer-divertor and roof-baffle samples. Only at the upper divertor and on certain limiter samples close to the puffing valve, the intensity level of the ^{13}C signal in the topmost 50-nm layer was comparable to that recorded from inner-divertor samples in figure 5.

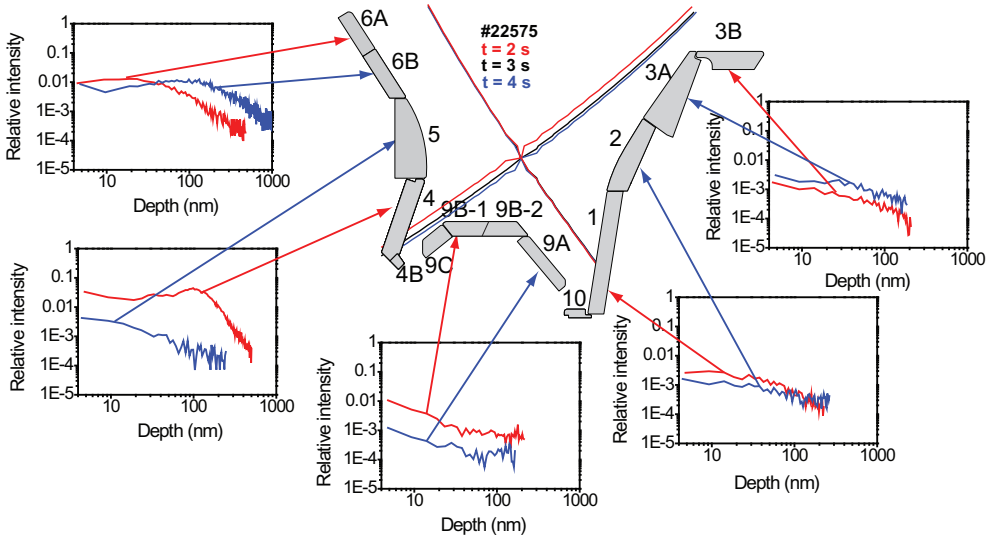

Figure 5. Examples of ^{13}C depth profiles measured from W-coated lower-divertor tiles. The ^{13}C signal is normalized to that of W. The arrows and colours indicate the approximate locations from which each profile was recorded. Also the separatrix at different times (red = 2 s, black = 3 s, blue = 4 s) during the flat-top phase of the discharge #22575 is shown.

In all the profiles, part of the signal results from natural ^{13}C deposited together with ^{12}C during a longer period, but this additional ^{13}C source has only a minor contribution to the depth profiles and the extracted ^{13}C densities. It should also be noted that the inner strike-point position was drifting during the discharges of the experiment as can be observed from the separatrix curves in figure 5. This drifting might have affected the measured deposition profiles and also the amount of ^{13}C, especially in tiles 4 and 9C.

In figure 6, the integrated surface density (in at/cm^2) of ^{13}C as a function of the s coordinate is shown, in part (a) for the whole lower divertor and in part (b) for all the analyzed tiles. Also a histogram of the the inner and outer strike-point times during the 12 discharges is presented in the figure. The data show that the deposition is largest at the inner-divertor tiles 6A and 6B and close to the strike-point areas of tile 4 but even in these tiles the ^{13}C amounts are rather small (typically $< 10^{16}$ at/cm^2) except for the inner strike point at $s \approx 500$ mm. The ^{13}C density then gradually decreases when moving from the inner to the outer parts of the divertor where the deposition is one or even two orders of magnitude smaller than at the inner divertor. A sharp decrease in the ^{13}C density is observed when going from tile 6B to tile 5. This is rather unexpected since the transition between these tiles is rather smooth. It can partly be explained by a rougher surface of tile 6B: the determined R_a values are $600 - 700$ nm for tiles 6A and 6B and $350 - 500$ nm for all the other W-coated divertor tiles. According to the observations of Ueda *et al* [41], the deposition of carbon is enhanced with the roughness of the W surface but also shadowing at the transition point could play a role in the accumulation of carbon on the surface.

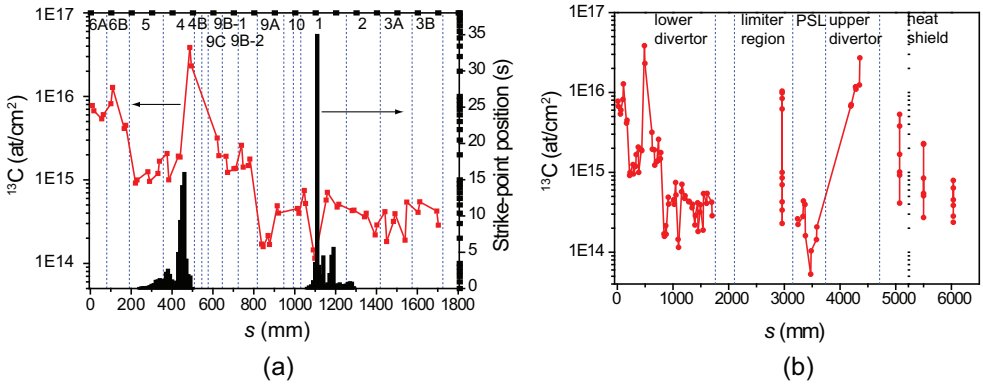

Figure 6. Surface density of ^{13}C (at/cm^2) on W-coated tiles as a function of the poloidal s coordinate in (a) lower-divertor areas and (b) around the whole torus. The acronym PSL denotes the passive stabilizer loop. In part (a), also a histogram for the inner (tiles 4 and 5) and outer (tile 1) strike-point times during the 12 discharges as a function of the s coordinate is presented.

In the main chamber (see figure 6b), equally small amounts of ^{13}C as in the outer divertor can be seen except in the before-mentioned areas at the upper divertor and locally in the upper parts of the heat shield and in the limiter region next to the puffing valve. However, on the uppermost heat-shield tile ($s \approx 5000$ mm) arc tracks were observed due to which the determined ^{13}C densities are not necessarily directly comparable to those taken from other heat-shield tiles, where by visual inspection the coating and the deposited layer were more intact.

The integrated amount of ^{13}C atoms in lower-divertor tiles is approximately 4.2×10^{20}, which corresponds to less than 1.5% of the total number of injected ^{13}C atoms (see table 1). This value was obtained by assuming toroidally symmetric deposition and performing toroidal and poloidal integration over the whole divertor region; the calculated ^{13}C surface densities in figure 6(a) were used for all the values of the s coordinate between two successive measurement points. The assumption of toroidal symmetry in ASDEX Upgrade has not been fully confirmed but observing anomalous toroidal deposition patterns for ^{13}C is unlikely. This is due to the fact that the injection valve for methane is located relatively far away from the plasma and, as a result, the incoming gas jet has a large surface area (port area $\approx 600 \times 1000$ mm^2) and is evenly distributed when it strikes the plasma. This results in more or less symmetric deposition toroidally since even small differences in the radial penetration of particles in the SOL lead to different flux tubes which are toroidally connected to very different areas.

Part of the injected ^{13}C was deposited in the main chamber as can be seen in figure 6(b). As in the lower-divertor case above, we obtained the following estimates for the deposition in different main-chamber areas: limiter tiles 0.3%, upper divertor 6%, heat shield 0.6%, and PSL 0.04%. The upper-divertor value (6%) is, however, somewhat uncertain since only one tile from that region was removed for post mortem analyses. If the deposition profile at the upper divertor was more like that close to the inner strike

zone, i.e., the high surface densities measured around $s \approx 4200$ mm represented a local peak similarly to tile 4 in the inner divertor, then only around 1% of the injected ^{13}C would have ended up on the top parts of the vessel. This is not totally unlikely: from figure 4 one observes that a secondary separatrix appears just next to the analyzed upper-divertor tile. The deposition at the upper divertor therefore ranges between 1% and 6%.

SIMS analysis of silicon samples mounted below the tiles 9C and 9A of the roof baffle indicated strong deposition in these regions: the determined surface densities were typically $10^{16} - 10^{17}$ at/cm^2 with the highest values at the high-field side of the vessel. Due to a different substrate material, these numbers are not directly comparable to the data in figure 6 but, nevertheless, they give a correct order-of-magnitude estimate for the ^{13}C studies. In the immediate vicinity of the injection valve, the deposition of ^{13}C on silicon samples was much smaller (surface densities $< 5 \times 10^{15}$ at/cm^2). This is in accordance with the fact that close to the injection point the puffed gas is still neutral and only after it has interacted with plasma and dissociated or ionized in the limiter region, deposition can take place. Based on these results, we obtained that approximately 1% of the injected ^{13}C has been deposited below the roof baffle and only 0.07% around the injection port. These results are comparable to the results in [19] where 0.6–0.8% of the injected deuterium was found below the roof baffle.

3.2. ^{13}C on uncoated areas of marker tiles

The deposition pattern of ^{13}C on the uncoated graphite areas of marker tiles is markedly different from that on W-coated tiles, see figure 7. Here the surface density of ^{13}C as a function of the s coordinate is shown together with the results of figure 6(a). The deviation of the two curves from each other is especially large in the outer divertor: the surface densities on the W-coated tiles are a factor of 10 or even 100 smaller. Furthermore, the ^{13}C distribution for the graphite areas has two prominent peaks close to both the inner (tiles 4 and 4B, $s \approx 500 - 550$ mm) and the outer strike points (tile 1, $s \approx 1100 - 1200$ mm). Such a feature cannot be identified in figure 6. Even more interesting is that the sharp transition between the ^{13}C surface densities on tiles 6B and 5 (see previous subsection) cannot be observed. As discussed above, surface roughness may explain this behaviour: the average surface roughness of the analyzed graphite samples is similar ($R_a \approx 250 - 350$ nm) for most of the marker tiles; samples from tiles 5 and 1 have somewhat rougher surfaces ($R_a \approx 350 - 400$ nm for tile 5 and $R_a \approx 500 - 600$ nm for tile 1).

If the whole lower divertor consisted of carbon tiles, then on the basis of figure 7, the estimated number of ^{13}C atoms in the lower-divertor regime would be 1.8×10^{21} corresponding to 7% of the puffed atoms. This observation is consistent with earlier results in [24, 25], also obtained from uncoated stripes of marker tiles prepared for the 2002/2003 and 2004/2005 campaigns when the divertor strike zones were still made of graphite.

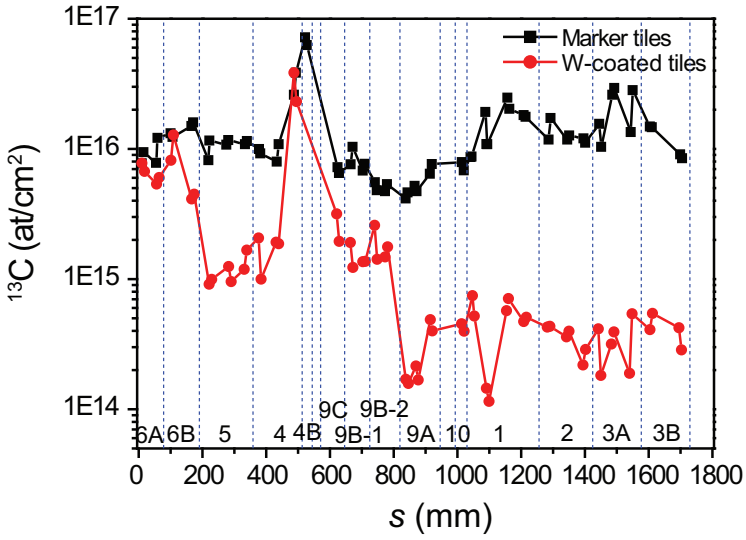

Figure 7. Surface density of ^{13}C (at/cm^2) as a function of the poloidal s coordinate in the lower divertor for the uncoated graphite areas of marker tiles (black squares) and W-coated tiles (red circles).

Depth profiles from three samples, from the inner strike-point tile 4 ($s \approx 490$ mm), from the outer strike-point tile 1 ($s \approx 1160$ mm) and from the roof-baffle tile 9A ($s \approx 870$ mm), are shown in figure 8. The figure shows that in the uncoated areas of the marker tiles ^{13}C has accumulated in a 100–200 nm thick surface layer; this is the general tendency for all the marker tiles in the lower divertor. Only in the immediate vicinity of the inner strike point (figure 8(a)) and in tile 6B, the ^{13}C signal extends down to 500 nm but again the largest contribution comes from the 10–50-nm thick surface layer. The analysis was somewhat complicated by tungsten re-deposited on the originally uncoated stripe, and the thickness of this layer ranged from a few nanometers in the roof-baffle tiles to almost 100–200 nm in tiles 1 and 4 (see figures 8(a) and (b)). In many of the samples, W was therefore present — but with decreasing intensity — practically to the same depth as the ^{13}C signal and even beyond.

3.3. Comparison with ^{13}C results from previous campaigns

In figure 9, the lower-divertor results of figure 7 are compared to the published data from the 2003 and 2005 campaigns [24, 25]. The ^{13}C surface densities are normalized to the number of injected ^{13}C atoms (see table 1). The deposition patterns of ^{13}C on carbon (2003, 2005, and marker tiles in 2007) are more or less symmetric between the inner and outer divertor, and especially in the outer divertor the three curves are very similar. In the inner divertor, the 2003 curve, resulting from an H-mode experiment, exhibits large variations from tile to tile and has a peak in tile 6A; the 2005 and 2007 profiles remain almost in a steady level. In addition to the different plasma conditions used in the experiments, the slighly modified shapes of tiles 5 and 4 before the 2007

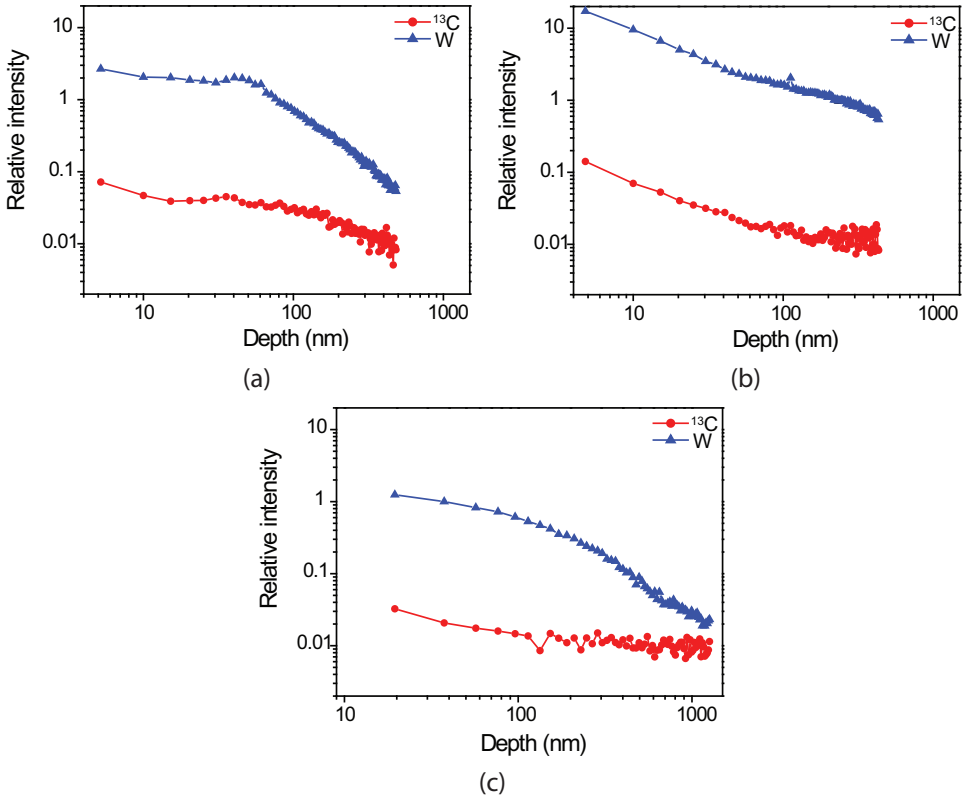

Figure 8. Examples of ^{13}C depth profiles measured from uncoated areas of (a) the inner-divertor tile 4 (close to the inner strike point, $s \approx 490$ mm), (b) the outer-divertor tile 1 ($s \approx 1160$ mm), and (c) the roof-baffle tile 9A ($s \approx 870$ mm). Also the W profiles on the same tiles are shown. Both the ^{13}C and W data are presented relative to ^{12}C. In (a) and (b), having a noticeable layer of re-deposited tungsten on them, the sputtering rate of the W coating has been used to convert the measurement time to depth. For the profile in (c), the sputtering rate of carbon was chosen.

campaign may have contributed to the inner-divertor deposition profiles. The two L-mode data sets (2005 and 2007) in figure 1 show that the electron temperature T_e was higher in the inner divertor in 2007, and thus less net deposition is expected to take place there. Unfortunately, due to a lack of SIMS measurement points from tile 4 in 2005, this conclusion cannot be verified.

The most interesting observation is that the poloidal ^{13}C deposition profile of the W-coated 2007 tiles is entirely different from all the other profiles, in particular along the outer parts of the divertor. This suggests that the different wall material changes radically the deposition behaviour of carbon, an effect already observed in TEXTOR [39, 40]. The surface roughness is not expected to play a large role since the variations between the measured R_a values from neighbouring tiles were not large and, furthermore, the W-coated tiles were generally rougher than the uncoated graphite stripes of the marker tiles. In addition, since the marker tiles and the W-coated tiles originated from almost the same toroidal location, toroidal asymmetry cannot explain

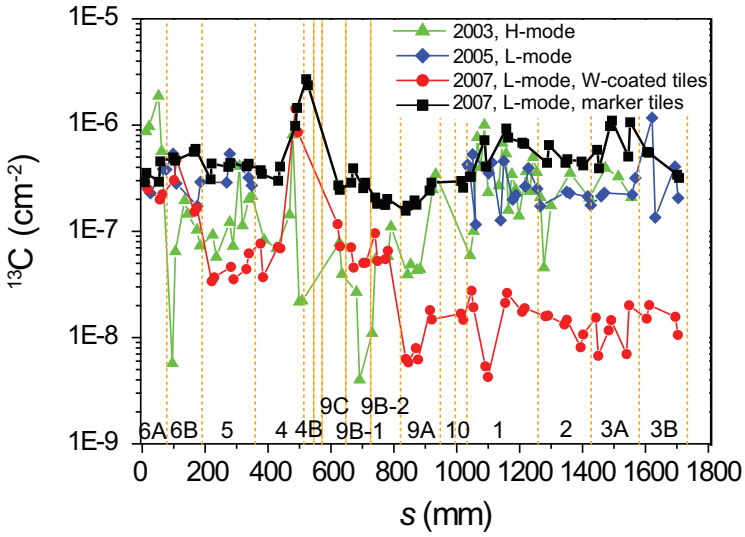

Figure 9. Deposition of ^{13}C in lower divertor measured after the injection experiments in 2003 (green triangles), 2005 (blue diamonds), and 2007 from uncoated areas of the marker tiles (black squares) and from W-coated tiles (red circles). The measured surface densities have been divided by the number of atoms injected.

the determined differences in roughness or the measured ^{13}C densities.

3.4. DIVIMP modelling of the 2007 experiment

The impurity Monte-Carlo code DIVIMP [31] was used to simulate the scrape-off layer, as well as the injection, transport, and deposition of ^{13}C in the low-density L-mode plasma of the 2007 experiment. The magnetic equilibrium was taken from the ASDEX Upgrade discharge #22575. The background plasma parameters for the deuteron density and temperature, the deuteron flow velocity, and the potential and electric field were calculated by using the onion-skin method (OSM, option 22) [42, 43]. The profiles for the electron density and temperature at the inner and outer target plates, derived from the Langmuir-probe data, were used as inputs (see figure 10(a) and (b)). At the outer midplane, the calculated electron density and temperature profiles have been compared with the measured profiles, extracted from the Lithium beam, ECE radiometer, and Thomson scattering measurements. The calculated electron density in the SOL matches with the experimental data within a factor of two while the calculated electron temperature is roughly two or three times higher (figure 10(c) and (d)). In addition, the blue curve in figure 10(d) shows a local peak in the SOL just outside the separatrix. This is due to the target profiles used by OSM: at the target, T_e has a radial peak outboard of the strike point (figure 10(b)). The calculated flow velocities, expressed as their Mach numbers, M, in figure 10(e), peak at the inner and outer targets where the Mach number approaches $M = 1$. The Mach number is defined as the ratio

of the flow velocity $v_\parallel$ in the direction parallel to B and the local ion sound speed, i.e.,

$$M = \frac{v_\parallel}{\sqrt{\left[k_\mathrm{B}\left(T_\mathrm{e} + T_\mathrm{i}\right)\right]/2m_\mathrm{i}}}, \tag{1}$$

where m_i is the hydrogen mass, T_i is the ion temperature, and k_B the Boltzmann constant. Upstream from the targets, the calculated Mach number decreases to zero; between the inner and outer midplane regions the flow in the SOL is stagnant. This is in contradiction to the measured flow velocities from various tokamaks at different poloidal locations [44], but modelling the flow correctly is a real challenge even to more sophisticated fluid codes [45, 46].

^{13}C ions with a charge state of +1 were launched in the SOL at the outer midplane and their trajectories were followed until they exited the calculation grid. Also impact ionization with electrons and different recombination processes were taken into account in the simulations. The injection point was systematically varied in the radial direction from zero (at the separatrix) to 13 mm (in the far SOL). An initial energy of 0.3 eV, corresponding to an average Franck–Condon energy of the CH radicals, was assumed together with an isotropic source distribution. Spatially constant diffusion coefficients were used in this study for ^{13}C ions in all their charge states, and their values were varied from 0.1 to 2.0 m^2/s. Due to a radially limited calculation grid, a finite probability for the ions to re-enter the plasma was considered. The grid was artificially extended into the halo plasma by using an option built into DIVIMP, and this extension ranged from 0 to 5 cm. In that region, only perpendicular transport occurs and impurity ions can either diffuse back into the SOL plasma or to the walls. Furthermore, ^{13}C is counted for deposition only, and not re-launched to simulate re-erosion or recycling.

The DIVIMP simulations generally show that almost 90% of the injected ^{13}C is deposited on the passive stabilizer loop, the upper divertor, and the limiter region. This pattern remains qualitatively the same over a wide range of simulation parameters. The calculated deposition on the main parts of the wall is shown in table 2 for the case where ^{13}C was injected at 5 mm outside the separatrix, the diffusion coefficient was 0.5 m^2/s, and the grid was extended by 2 cm. This result is qualitatively consistent with the strong deposition measured on one W-coated tile in the upper divertor as shown in figure 6(b). In contrast to the measurements, virtually nothing is deposited in the lower divertor. When moving the injection point of ^{13}C away from the separatrix and increasing the diffusion coefficient, the outer midplane becomes the dominant region for deposition.

The calculated deposition pattern is due to the gradient force, related to the ion temperature, pointing toward the top of the plasma in both the inner and outer main SOL (see figure 10(f)). This force pushes the ^{13}C ions toward the top of the vessel. The simulations show that the ^{13}C ions mainly reach the heat shield via the main plasma. Since the plasma is calculated to be stagnant for most of the SOL between the inner and outer midplane, ^{13}C accumulates at the top and is subsequently deposited onto the grid edge representing the upper divertor. Imposing a plasma flow of $M \sim 0.5$ from the outer midplane toward the inner divertor, as done by Elder *et al* for DIII-D [33], the ^{13}C ions are likely to be swept with the background plasma toward the inner divertor,

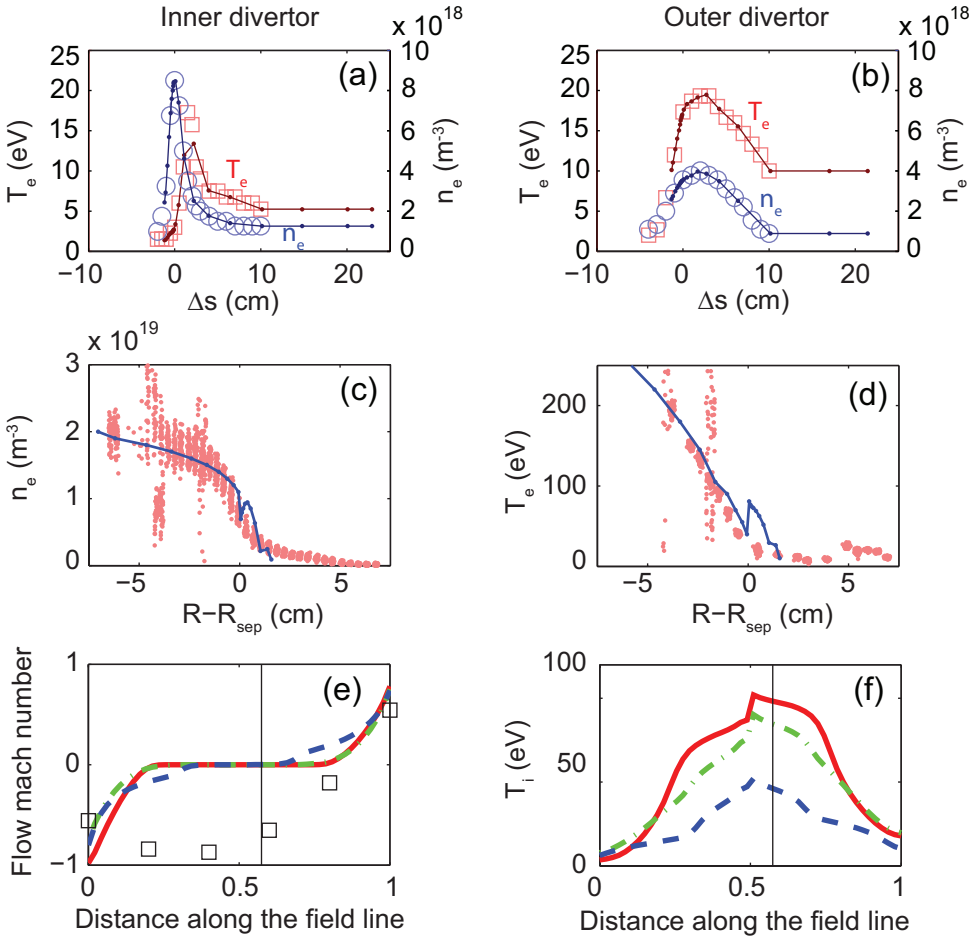

Figure 10. (a,b) Measured electron temperature (T_e, red squares) and density (n_e, blue circles) profiles along (a) the inner strike-point and (b) the outer strike-point region for the ASDEX Upgrade discharge #22575. The solid lines represent the DIVIMP input. (c) Radial n_e profile as a function of distance from the separatrix at the outer midplane. (d) Radial T_e profile at the outer midplane. The solid blue lines are the calculated densities and temperatures from DIVIMP. (e) Parallel-B flow velocities for three different radial locations in the SOL: red = 0.3 mm, green = 3.3 mm, and blue = 13.1 mm radially outside the separatrix. The black open squares represent an ansatz for the poloidal flow profile as published in [44]. The vertical line highlights the puffing location, the coordinate value 0 corresponds to the inner divertor, the value 1 to the outer divertor, and 0.5 denotes the top of the vessel. (f) Parallel-B profile of the SOL ion temperature, colour codes and labellings are the same as in (e).

and do not accumulate at the top. Such prescriptive work is not within the scope of this paper.

4. Long-term deposition studies

The deposition behavior of carbon was also studied by recording the depth profile of ^{12}C down to a depth of approximately 3–5 μm in the same W-coated samples used for

Table 2. DIVIMP results of the deposition of ^{13}C on various regions of ASDEX Upgrade for shot #22575. In these simulations, singly ionized ^{13}C was injected 5 mm outside the separatrix, and a spatially constant diffusion coefficient of 0.5 m^2/s was used. The experimental ^{13}C results are summarized here for comparison (see section 3.1 for details). In the first column, the results are normalized to the total number of ^{13}C atoms injected, while in the second column the results are normalized to the number of ^{13}C atoms found experimentally.

	W-coated tiles (normalized to the amount of ^{13}C injected)	**W-coated tiles (normalized to the amount of ^{13}C found)**	**DIVIMP**
Inner divertor	0.8%	10%	0%
Outer divertor	0.1%	1%	0%
Limiter area	0.3%	4%	30%
PSL	0.04%	0.5%	18%
Upper divertor	< 6%	< 75%	38%
Heat shield	0.6%	8%	14%

the surface-density studies of ^{13}C. The analyses concentrated on lower-divertor samples; only a few samples from the main chamber were profiled, mainly to investigate the similarities and differences between the depth profiles in the divertor and other regions. A coarser mass resolution of $m/\Delta m \approx 300$ was now used: for the overall deposition studies high-resolution measurements do not provide any additional information. At the depth of the selected 3–5 μm, the primary ions had penetrated their way through the PVD coating or the carbon signal had decreased to its background level in the VPS coating.

Examples of the depth profiles of carbon, from the inner divertor tile 6B and the outer divertor tile 3A, are shown in figure 11. Also the depth profiles of hydrogen (H), deuterium (D), boron (B), and tungsten (W) are drawn in the figure. Although boronizations were not done in ASDEX Upgrade in 2007, remnants of boron from previous campaigns were observed on the surface of many samples, and in some cases there was a 10–100 nm thick boron- and/or carbon-rich layer on top of W. The ^{13}C profiles in figure 11 include also the contribution from such isobars as $^{12}CH^+$ and thus give the true ^{13}C surface density only when the hydrogen signal has reached the noise level.

Carbon is deposited in an approximately 500-nm thick layer on the coatings (see figure 11). Also deuterium is mainly retained in this deposited layer. The point halfway between the depth values where the intensity of ^{12}C raises from its background value to a new maximum and the W signal has started to go down marks the thickness of the W coating. In the examples of figure 11, the thicknesses of the coating are 2.5 μm and 2.2 μm, well in accordance with the nominal values for the PVD films on these tiles (3 μm). No noticeable differences were observed between the depth profiles of ^{12}C from inner- and outer-divertor tiles. In the main chamber, the shape of the measured profiles was generally similar to those obtained from the lower-divertor samples but the surface

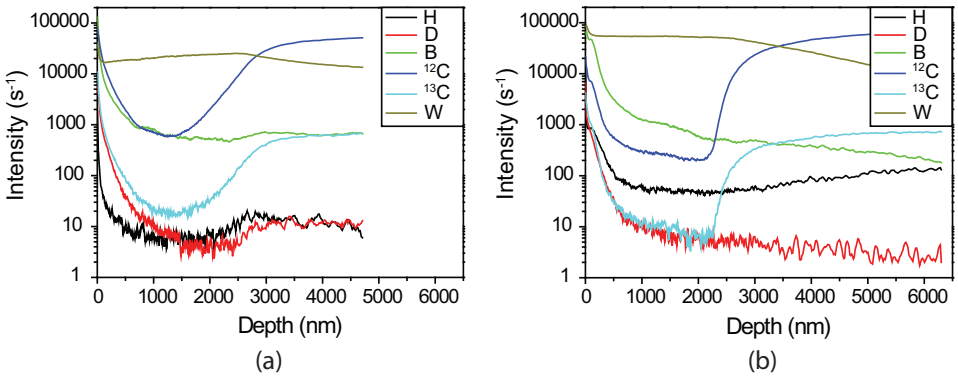

Figure 11. SIMS depth profiles from the W coating of (a) the inner-divertor tile 6B and (b) the outer-divertor tile 3A.

densities of the studied elements were different.

The integrated amount of carbon (^{12}C) on W as a function of the s coordinate in the divertor area is shown in figure 12. Also the published NRA data [18] from the same tiles, measured using 2500-keV ^{3}He ions, is reproduced here. The SIMS data has been scaled to the surface density of ^{12}C (in at/cm^2), quantitatively measured with NRA, at the inner strike zone (tile 4). The deposition of carbon is found to peak close to the inner strike point in tile 4 and in the innermost divertor tiles 6A and 6B. This is in accordance with the ^{13}C data in figure 9. The sudden drop in the carbon inventory, recall figure 6, when moving from tile 6B to tile 5 can be clearly seen as well. In addition, the SIMS results show a smaller but still discernible peak at the outer divertor, in tiles 1 and 2. From the NRA curve, this peak can also be identified albeit it is much weaker. A possible explanation for this discrepancy are strong variations, of the order of $2-3\times10^{17}$ at/cm^2, in the integrated C contents for data points with the same s coordinate in these tiles; for the rest of the tiles, the error bars are 3–5 times smaller. Large error bars can easily lead to exaggeration of the amount of carbon on the samples. However, equally well the reason could lie in the inhomogeneous surface of the tiles and the different spot sizes of the ion beams used in NRA and SIMS: the SIMS spot (300×430 μm^2) is much smaller than the NRA spot (diameter about 1.8 mm). If carbon is locally concentrated in pits of a rough surface, it is more likely to be observed with SIMS than with NRA. Unfortunately, the SEM investigations of the surfaces of tiles 1 and 2 did not give a definitive conclusion to this problem. The VPS coating of tile 1 had lots of craters as well as all kinds of droplets and surface features on it, which explains the variations in the determined ^{12}C concentrations. However, although the surface of the PVD coating on tile 2 had holes on it in the scales < 200 μm, we have no information on the elemental composition of the peaks and valleys of the surface; the carbon signal could not be distinguished from the dominating W signal with the SEM that we used. Explaining the difference between the NRA and SIMS curves is thus a topic of future studies.

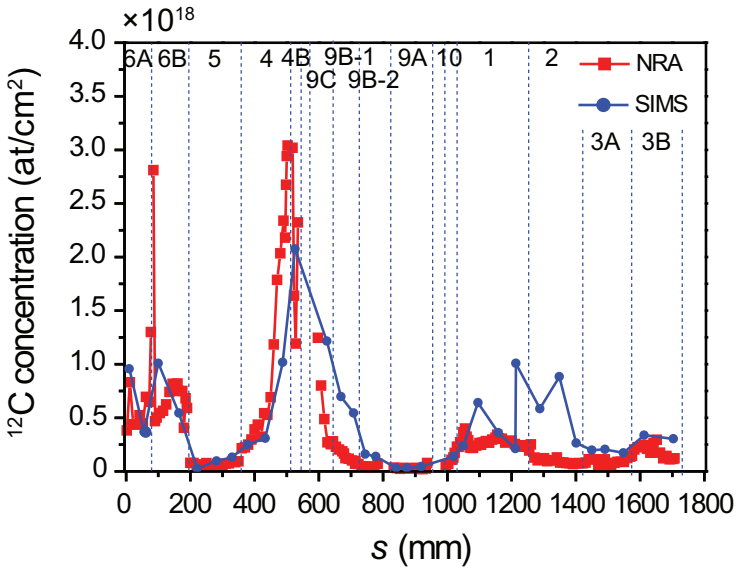

Figure 12. Integrated amount of carbon (^{12}C, in at/cm^2) in the W coatings of the analyzed W-coated tiles. The NRA results are marked with red squares and the SIMS results with blue circles. The SIMS data has been scaled to match with the absolute values given by NRA measurements in the inner divertor.

Our results support the conclusions [18] that the inner divertor is deposition dominated. We also determined the poloidal deposition profile of D in the divertor regions, and it was qualitatively similar to figure 12: deposition peaks were observed in tiles 6A and 6B and close to the inner and outer strike points in tiles 4, 9C, and 1. This implies that deuterium is co-deposited with carbon on tungsten and is in agreement with the data of Mayer *et al* [18] although there the outer-divertor peak was attributed to D trapped in W. In the main chamber, deposition plays a large role only in the upper heat shield and at the upper divertor; these are regions where ^{13}C was also found to have accumulated.

5. Discussion and conclusions

In this article, we have studied the migration and deposition of ^{13}C in ASDEX Upgrade by injecting $^{13}CH_4$ into the torus in the end of the 2007 experimental campaign. The surface density of ^{13}C was determined from a full set of lower divertor tiles and selected main-chamber tiles. The injection was accomplished from a valve installed at the outer midplane, toroidally displaced about 45 degrees from where the tiles were retrieved. The tiles had standard PVD or VPS tungsten coatings on them, and the analyses were made using SIMS. In addition, another complete set of divertor tiles from a neighbouring cross section of sector 11, equipped with uncoated marker stripes, was measured to compare the deposition patterns on carbon and on tungsten.

On the W-coated tiles, the ^{13}C surface densities were larger in the inner than outer

parts of the divertor. In fact, in the outer divertor and roof baffle, ^{13}C was barely distinguishable from the background level on many of the analyzed tiles. The main deposition peaks occurred on tiles 4 (inner strike-point tile) and 6A and 6B (located in the innermost upper corner of the divertor) but generally the deposition was much smaller than what had been measured after previous ^{13}C injection experiments in 2003 and 2005: only 1.5% of the injected ^{13}C atoms were estimated to have been deposited in the divertor compared to 7.1% in 2003 and 8.9% in 2005 [24, 25]. In the main chamber, the deposition on the studied tiles was as weak as on the outer divertor tiles except on a limiter tile close to the injection valve, in the upper parts of the heat shield and in the upper divertor where we estimated that 1–6% of the injected ^{13}C had accumulated. This suggests that part of ^{13}C atoms was transported along field lines into these regions or travelled in the form of injected methane molecules. This conclusion is supported by the DIVIMP simulations, according to which especially the upper divertor is a strong deposition area (38% of the deposited ^{13}C).

Although the sinks for the missing ^{13}C could not identified yet, there are a few processes which could be potential candidates. First of all we can exclude a strong deposition close to the injection valve since only 0.07% of the puffed gas was found on the silicon wafers located in the injection port. However, part of the injected methane could have been pumped out from the torus without any deposition taking place — cryopumps in ASDEX Upgrade are effective in pumping methane — but detailed measurements to support this hypothesis are missing. Methane may have also leaked from the injection valve directly to the vacuum pumps without ever being in contact with plasma. Another possible sink is deposition in remote areas and gaps between the tiles. Analyses of silicon samples mounted below the roof baffle have already revealed some strong sinks for carbon there, and this research will be continued in the future. Furthermore, one has to take into account that the deposition of ^{13}C largely depends on the location of the injection valve and the geometry of the tokamak. For example, in DIII-D approximately 30–40% of the puffed ^{13}C has been observed to deposit in the lower divertor and 10% close to the injection point [30] but there the injection was toroidally symmetric and the injection valve was located closer to the plasma and further to the high-field side than in ASDEX Upgrade. As already discussed in section 3, toroidally asymmetric deposition is not expected to play a large role.

All the aspects discussed above will be investigated in forthcoming injection experiments. Particular attention will be paid to the composition of the residual gas during and after the injection of ^{13}C, to the deposition in gaps and remote areas as well as to the toroidal symmetry of the deposition.

As mentioned above, after the 2003 and 2005 experiments the lower divertor areas were estimated to contain 7–9% of the injected tracer atoms, so the transition to a full-W machine in 2007 has had a large effect on the overall deposition behaviour. The measured ^{13}C deposition profiles qualitatively match with the long-term carbon deposition patterns in ASDEX Upgrade [18, 19] and in JET [20, 21]: the inner divertor is a net deposition area and the strike-point region at the outer divertor is a net erosion

area. We also observed this to be the case by measuring the total amount of deposited ^{12}C in the W-coated tiles selected for ^{13}C analysis (see figure 12).

The deposition of ^{13}C on uncoated areas of the marker tiles, used to investigate deposition on graphite, was markedly different from the case of W-coated tiles. First of all, equally strong deposition occurred on the inner- and outer-divertor tiles with two prominent peaks in both strike-point tiles (tiles 1 and 4) in the case of graphite surfaces. Secondly, the surface densities of ^{13}C on these tiles were significantly larger than on the corresponding W-coated tiles and to a large degree comparable to the values determined after the 2003 and 2005 experiments. The reasons for the large deviations between two similar sets of tiles appear to be the result of the different substrate material: carbon is deposited differently on tungsten than on carbon. At the inner divertor, the substrate effect is not as prominent as at the outer divertor or at the roof baffle. This can be explained by the fact that the inner divertor is a deposition-dominated region. In this zone, the incoming ^{13}C atoms were thus deposited on top of a carbon-rich layer independent of the material underneath.

The observation of carbon depositing differently on W and on C is supported by the surface-roughness measurements, which showed that the variations in roughness between neighbouring tiles, both for the W-coated and marker tiles, were not large and the marker tiles even showed a smoother surface than the W-coated ones. As discussed in refs. [39–41], in that case it is the substrate material that has the largest effect on the deposition efficiency of carbon: a value of 4% has been determined for graphite and 0.3% for tungsten substrates in TEXTOR. Local re-erosion and re-deposition, possibly in several successive steps [35] have been suggested to play a large role in the migration of carbon from tile to tile in the scrape-off layer plasma. The re-erosion of carbon from a tungsten surface is probably larger than from graphite, especially in the outer divertor, or the differences in surface chemistry dominate the deposition there. At least the deposition asymmetry between the inner and outer divertor for the W-coated tiles can be explained by re-erosion since the eroding fluxes are usually smaller at the inner than outer divertor.

The reasons for the different erosion of a thin deposited layer from tungsten and carbon surfaces has been discussed in refs. [39, 47]. The enhanced erosion of a thin film from a tungsten substrate is attributed to a larger recoil of plasma particles from a heavy element, which leads to a higher probability to physically sputter a carbon atom from the surface. This mechanism could well explain the large deviations in the ^{13}C curves in figure 7 in the outer divertor: here the deposited films are thinner than in the inner divertor and thus easily sputtered as a result of plasma exposure. Close to the inner strike point the deposited layers are thick, and the incoming ^{13}C atoms cannot distinguish the surface from a bulk substrate. The identification of physical mechanisms behind erosion and migration of ^{13}C is currently being done and the results will be reported later. For the final verification of the conclusions presented in this article, a new ^{13}C experiment in ASDEX Upgrade with the same plasma parameters as in 2005 is considered.

Acknowledgements

This work, supported by the European Communities under the contract of Association between Euratom and Tekes, was carried out within the framework of the Task Force on Plasma Wall Interactions of the European Fusion Development Agreement. The views and opinions expressed herein do not necessarily reflect those of the European Commission.

A.H. thanks Helsinki University of Technology for a post-doctoral grant and T. K.-S. the Academy of Finland, project number #121371, for financial support. The authors thank E. Haimi from the Department of Materials Science and Engineering of Helsinki University of Technology for the electron microscope analyses.

References

[1] Federici G, Brooks J N, Coster D P, Janeschitz G, Kukushkin A, Loarte A, Pacher H D, Stober J and Wu C H 2001 *J. Nucl. Mater.* **290–293** 260
[2] Bolt H, Barabash V, Federici G, Linke J, Loarte A, Roth J and Sato K 2002 *J. Nucl. Mater.* **307–311** 43
[3] Federici G *et al* 2003 *J. Nucl. Mater.* **313–316** 11
[4] Federici G *et al* 2001 *Nucl. Fusion* **41** 1967
[5] Pitts R A *et al* 2005 *Plasma Phys. Control. Fusion* **47** B303 b
[6] Roth J *et al* 2008 *Plasma Phys. Control. Fusion* **50** 103001
[7] Loarer T *et al* 2007 *Nucl. Fusion* **47** 1112
[8] Rubel M, Cecconello M, Malmberg J A, Sergienko G, Biel W, Drake J R, Hedqvist A, Huber A and Phillips V 2001, *Nucl. Fusion* **41** 1087
[9] Matthews G F *et al* 2007 *Phys. Scr.* **T128** 137
[10] Neu R *et al* 2007 *J. Nucl. Mater.* **363–365** 52
[11] Neu R, Dux R, Kallenbach A and ASDEX Upgrade Team 2008 *J. Phys. Conf. Series* **100** 062001
[12] Dux R *et al* 2009 *J. Nucl. Mater.* **390–391** 858
[13] Neu R *et al* 2007 *J. Nucl. Mater.* **367–370** 1497
[14] Mayer M, Rohde V, Likonen J, Vainonen-Ahlgren E, Krieger K, Gong X, Chen J and ASDEX Upgrade Team 2005 *J. Nucl. Mater.* **337–339** 119
[15] Mayer M, Rohde V, Ramos G, Vainonen-Ahlgren E, Likonen J, Chen J L and ASDEX Upgrade Team 2007 *Phys. Scr.* **T128** 106
[16] Mayer M *et al* 2009 *Phys. Scr.* **T138** 014039
[17] Rohde V, Dux R, Mayer M, Neu R, Pütterich T, Schneider W and ASDEX Upgrade Team 2004 *Phys. Scr.* **T111** 49
[18] Mayer M *et al* 2009 *J. Nucl. Mater.* **390–391** 538
[19] Mayer M, Rohde V, Ramos G, Vainonen-Ahlgren E, Likonen J, Herrmann A, Neu R and ASDEX Upgrade Team 2007 *Nucl. Fusion* **47** 1607
[20] Coad J P, Bekris N, Elder J D, Erents S K, Hole D E, Lawson K D, Matthews G F, Penzhorn R-D and Stangeby P C 2001 *J. Nucl. Mater.* **290–293** 224
[21] Coad J P, Likonen J, Rubel M, Vainonen-Ahlgren E, Hole D E, Sajavaara T, Renvall T, Matthews G F and JET EFDA Contributors 2006 *Nucl. Fusion* **46** 350
[22] Pégourié B *et al* 2004 *Phys. Scr.* **T111** 23
[23] Pégourié B *et al* 2009 *J. Nucl. Mater.* **390–391** 550
[24] Vainonen-Ahlgren E, Likonen J, Renvall T, Rohde V, Neu R, Mayer M, Pugno R, Krieger K and ASDEX Upgrade Team 2005 *J. Nucl. Mater.* **337–339** 55

[25] Vainonen-Ahlgren E, Likonen J, Renvall T, Rohde V, Mayer M and ASDEX Upgrade Team 2007 *J. Nucl. Mater.* **363–365** 270
[26] Likonen J, Lehto S, Coad J P, Renvall T, Sajavaara T, Ahlgren T, Hole D E, Matthews G F, Keinonen J and JET EFDA Contributors 2003 *Fus. Eng. Des.* **66–68** 219
[27] Rubel M J, Coad J P, Stenström K, Wienhold P, Likonen J, Matthews G F and Phillips V 2004 *J. Nucl. Mater.* **329–333** 795
[28] Coad J P *et al* 2007 *J. Nucl. Mater.* **363–365** 287
[29] Wampler W R, Allen S L, McLean A G and West W P 2005 *J. Nucl. Mater.* **337–339** 134
[30] Wampler W R, McLean A G, Allen S L, Brooks N H, Elder J D, Fenstermacher M E, Groth M, Stangeby P C, West W P and Whyte D G 2007 *J. Nucl. Mater.* **363–365** 72
[31] Stangeby P C, Farrell C, Hoskins S and Wood L 1988 *Nucl. Fusion* **28** 1945
[32] McLean A G *et al* 2005 *J. Nucl. Mater.* **337–339** 124
[33] Elder J D *et al* 2005 *J. Nucl. Mater.* **337–339** 79
[34] Elder J D *et al* 2007 *J. Nucl. Mater.* **363–365** 140
[35] Strachan J D *et al* 2008 *Nucl. Fusion* **48** 105002
[36] Groth M *et al* 2007 *Phys. Plasmas* **14** 056120
[37] Xuereb A, Groth M, Krieger K, Kurki-Suonio T, Asunta O, Likonen J, Coster D P and ASDEX Upgrade Team 2010 *J. Nucl. Mater.* **396** 228
[38] Lehto S, Likonen J, Coad J P, Ahlgren T, Hole D E, Mayer M, Maier H and Kolehmainen J 2003 *Fusion Engineering and Design* **66–68** 241
[39] Kreter A *et al* 2006 *Plasma Phys. Control. Fusion* **48** 1401
[40] Kreter A *et al* 2008 *Plasma Phys. Control. Fusion* **50** 095008
[41] Ueda Y *et al* 2009 *J. Nucl. Mater.* **390–391** 44
[42] Stangeby P C *et al* 2003 *J. Nucl. Mater.* **313–316** 883
[43] Elder J D 2009 *DIVIMP options* (`http://starfire.utias.utoronto.ca/divimp/docs/divdocs.html` , accessed September 2009)
[44] Lipschultz B *et al* 2007 *Nucl. Fusion* **47** 1189
[45] Erents S K, Pitts R A, Fundamenski W, Gunn J P and Matthews G F 2004 *Plasma Phys. Control. Fusion* **46** 1757
[46] Groth M *et al* 2009 *Nucl. Fusion* **49** 115002
[47] Maier H, Schmid K and Eckstein W 2005 *J. Nucl. Mater.* **337–339** 480